

OFC Concludes with Almost 17,000 Individuals and 685 Exhibitors
 Read the closing press release on conference highlights.

- [Technical Digest Papers](#)
Download papers for technical talks.
- [View Session Recordings](#)
Watch technical sessions and show floor programs.
- [Be The First To Know](#)
Request OFC notifications.

Agenda of Sessions — Thursday, 03 April

	Rooms 201-202	Rooms 203-204	Rooms 205-206	Room 207	Room 208	Rooms 209-210	Rooms 211-212
07:30–16:30	Registration Open, South Lobby, Moscone Center						
8:00–10:00	Th1A • Machine Learning for Network Operations	Th1B • Weather Resilient Communications of the Future	Th1C • Optical Computing	Th1D • Coherent for Datacenters	Th1E • Advanced Modulator and Detectors	Th1F • Photonic Advancements for Scalable and Secured Networks	Th1G • Low Loss Passives
10:00–16:00	Exhibition, Halls A-F, (concessions available, coffee service 10:00–10:30)						
10:00–14:00	Unopposed Exhibit-only Time, Exhibition Halls A-F						
10:30–12:30	Th2A • Posters Session II, Room 303						
14:00–16:00	Th3A • Frontiers of Optical Network Architecture Summit – Network Architecture Evolution in the Age of AI	Th3B • What Building-to-Building Optical Interconnect Will Enable Gigawatt Scale Training Clusters?	Th3C • Ultra-Wideband Transmission	Th3D • Point to Multipoint and Satellite Networks	Th3E • Photo-Detector and Integration	Th3F • Fiber Sensing and Characterization	Th3G • Enabling Techniques for PON
16:00–16:30	Coffee Break, Level 2 Corridors						
16:30–18:30	Postdeadline Paper Sessions, Rooms 203-204, 205-206, 211-212, 213-214						

10:30 -- 12:30

Room 303

Th2A • Posters Session II

Th2A.1

A Reconfigurable 4- λ \times 25-Gb/s/ λ Silicon Ring-Resonator-Based WDM Receiver with Fast Wavelength Calibration, Jae-Ho Lee¹, Yongjin Ji¹, Hyun-Kyu Kim², Woo-Young Choi¹; ¹*Yonsei Univ., Korea (the Republic of)*; ²*Samsung Electronics, Korea (the Republic of)*. We present a reconfigurable 4- λ \times 25-Gb/s/ λ Si ring-resonator-based WDM receiver and, using it, demonstrate a new wavelength calibration technique that provides ring resonators with desired

Details as of 21 March 2025

Page | 134

All times in Pacific Time, UTC-07:00

2025 OFC Conference and Exhibition Session Guide

Disclaimer: this guide is limited to technical program with abstracts and author blocks as of 21 March 2025. For updated and complete information with special events, reference the online schedule or mobile app.

resonance wavelengths and maintains them against external temperature variation.

A Reconfigurable $4\text{-}\lambda \times 25\text{-Gb/s}/\lambda$ Silicon Ring-Resonator-Based WDM Receiver with Fast Wavelength Calibration

Jae-Ho Lee¹, Yongjin Ji¹, Hyun-Kyu Kim², and Woo-Young Choi^{1,*}

¹Yonsei University, 03722 Seoul, South Korea

²Formerly at Yonsei University when this work was done. Now at Samsung Electronics, Hwaseong, 18448 Gyeonggi-do, South Korea

*wchoi@yonsei.ac.kr

Abstract: We present a reconfigurable $4\text{-}\lambda \times 25\text{-Gb/s}/\lambda$ Si ring-resonator-based WDM receiver and, using it, demonstrate a new wavelength calibration technique that provides ring resonators with desired resonance wavelengths and maintains them against external temperature variation.
© 2025 The Author(s)

1. Introduction

As artificial intelligence and machine learning workloads increase, the interest in silicon photonic WDM optical links based on ring resonators is rapidly increasing [1]. On the receiver side, the cascaded ring resonator filters (RRFs) can de-multiplex wavelength division multiplexing (WDM) channels [2] with a small footprint and, if needed, provide the reconfiguration of the wavelength assignment. Various techniques have been used for implementing RRF-based reconfigurable WDM receivers [3-5]. The channel labeling strategy can be used [3], but it requires an additional modulator at the add port in the RRF. Operation in the electrical backend can be used [4], but with the increasing WDM channel number, its complexity can significantly increase. We previously reported a reconfigurable 4-channel Si RRF-based WDM receiver [5], but it required a substantial amount of wavelength calibration time. In this paper, we report a new 4-channel Si RRF-based WDM receiver and, using it, demonstrate a technique having much-reduced calibration time.

2. System implementation and wavelength calibration procedure

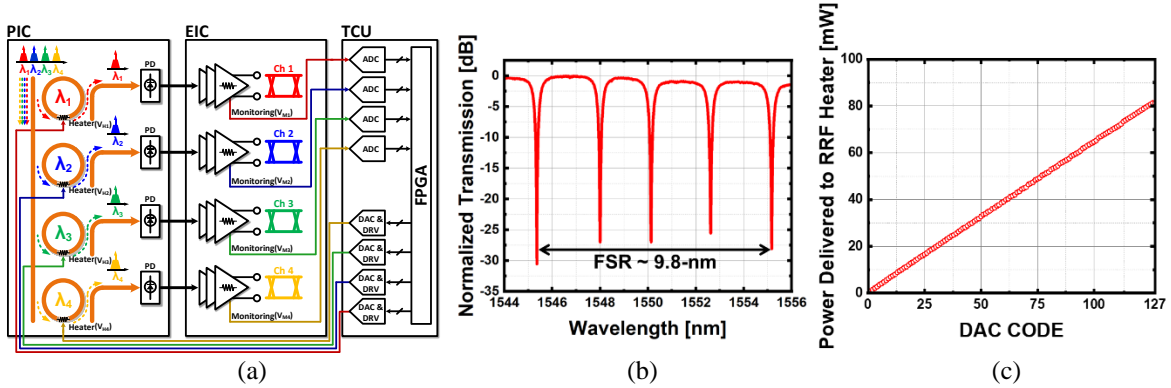


Fig. 1. (a) Block diagram of the WDM receiver with TCU. (b) Measured transmission spectrum of four RRFs and (c) power delivered to RRF heater.

Fig. 1(a) shows the block diagram of the WDM receiver with a temperature controller unit (TCU). The photonic IC (PIC) contains cascaded four RRFs having slightly different radii around $10\text{-}\mu\text{m}$ so that their resonance wavelengths are evenly spaced within one FSR as can be confirmed by the measured transmission spectrum in Fig. 1(b). The drop port for each RRF is connected to the integrated Ge photodetector (PD) whose output is wire-bonded to the TIA circuit within the electric IC (EIC) fabricated by 28-nm CMOS technology. Each TIA also provides the received power monitoring signal to the TCU consisting of ADCs, DACs with heater drivers, and an FPGA. The DAC is implemented so that it can provide the RRF heater power that linearly depends on the control code provided by the FPGA as can be seen by the measured data shown in Fig. 1(c).

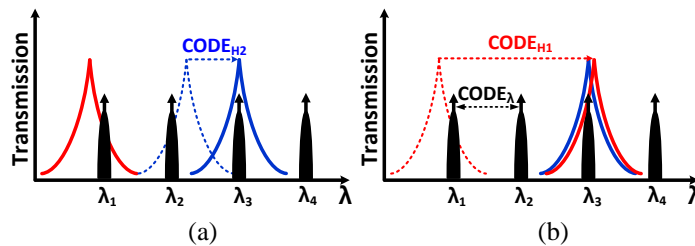


Fig. 2. Visualizations of (a) the first step and (b) the second step of the scan mode in the wavelength calibration technique of the TCU.

Since the resonance wavelengths of the four RRFs are evenly spaced, once the required DAC code difference for the WDM channel spacing between two RRFs is known and one of the RRF resonance wavelengths is aligned to one of the input wavelengths, then the TCU can easily determine all DAC codes required for all the RRF heaters. Fig. 2 schematically shows one example. Initially, when optical signals having four different input wavelengths are introduced to the receiver, the DAC code ($CODE_{H2}$) for the heater driver of the second RRF is swept so that its resonance wavelength is aligned to the adjacent input wavelength (λ_3) (Fig. 2(a)). When the resonance wavelength of this RRF is aligned with the λ_3 , the monitoring signal (V_{M2}) reaches its maximum value. Then, while maintaining $CODE_{H2}$, the DAC code ($CODE_{H1}$) for the heater driver of the first RRF, which is physically located before the second RRF within PIC, is swept to align its resonance wavelength to λ_3 (Fig. 2(b)). When the alignment is achieved, V_{M2} goes down since the λ_3 power is dropped into the first RRF before it reaches the second RRF. Then, the DAC code difference corresponding to the resonance wavelength spacing between RRFs ($CODE_{H1} - CODE_{H2}$) can be determined by the TCU and the DAC code difference corresponding to the wavelength spacing between input wavelengths ($CODE_\lambda$) can be determined in a similar approach. Finally, The TCU can produce the required DAC code for each RRF heater driver so that its resonance wavelengths are at the desired location. For any inaccuracies due to process variation as well as fluctuations due to external temperature variation, the TCU can perform proper compensation by the dithering technique [5].

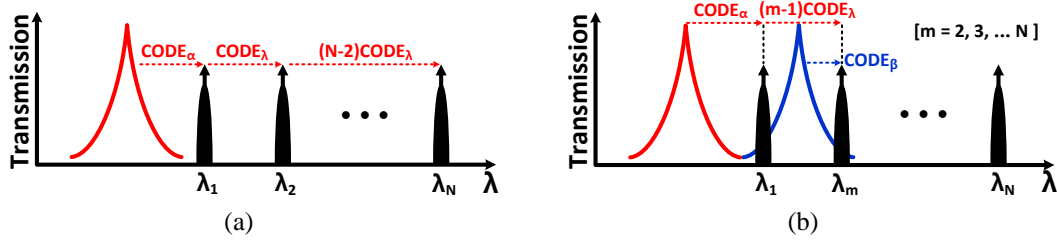


Fig. 3. Visualizations of (a) the scan mode reported in [5] and (b) the scan mode in the proposed calibration technique, in the case of N input wavelengths.

To compare the calibration time between the calibration technique reported in [5] and the proposed calibration technique, we compare the DAC codes required for the wavelength calibration in the case of N input wavelengths. Fig. 3(a) schematically shows the required DAC code to execute wavelength calibration by using a single RRF. $CODE_\alpha$ is required to align the resonance wavelength of the RRF with the adjacent input wavelength. $CODE_\lambda$ is required for the resonance wavelength of the RRF to be aligned with the next input wavelength. The code corresponding to $CODE_\alpha + (N-1)CODE_\lambda$ is required to sweep the RRF for the wavelength calibration. Fig. 3(b) schematically shows the required DAC code to execute the proposed wavelength calibration by using dual RRFs. $CODE_\alpha$ and $CODE_\beta$ are required to align the resonance wavelength of each RRF with the adjacent input wavelength. The code corresponding to $CODE_\alpha + CODE_\beta + (m-1)CODE_\lambda$ is required to sweep the RRFs for the wavelength calibration. The proposed calibration technique consumes a constant calibration time, regardless of the increase in the number of input wavelengths, and it becomes more efficient as the number of input wavelengths increases compared to [5]. Even if the initial input wavelength is positioned to the left of the resonance wavelength of the RRF, the subsequent Sort mode in the calibration enables accurate wavelength assignment.

3. Measurement results

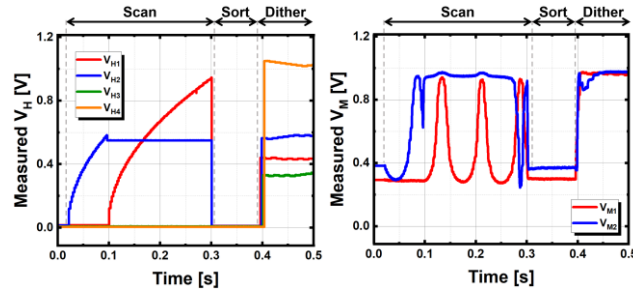


Fig. 4. Measured V_H and V_M of the TCU during the wavelength calibration.

To verify the operation of the receiver and TCU, the WDM optical input signals having four different wavelengths of $\lambda_1 = 1546.0$ -nm, $\lambda_2 = 1547.6$ -nm, $\lambda_3 = 1549.2$ -nm and $\lambda_4 = 1549.2$ -nm are coupled into the PIC. Due to the limitation in our measurement setup, only one WDM optical input signal can be modulated with 25-Gb/s, PRBS-7 data using a Mach-Zehnder modulator. Fig. 4 shows the measured heater control voltages (V_H) and monitoring signals (V_M) during the wavelength calibration. As can be seen, V_{H2} and V_{H1} are sequentially swept in the Scan mode, after which the TCU determines the required heater voltages for all the RRF heaters in the Sort mode and applies them with dithering in the Dither mode so that all the RRF resonant wavelengths are aligned to the input wavelengths.

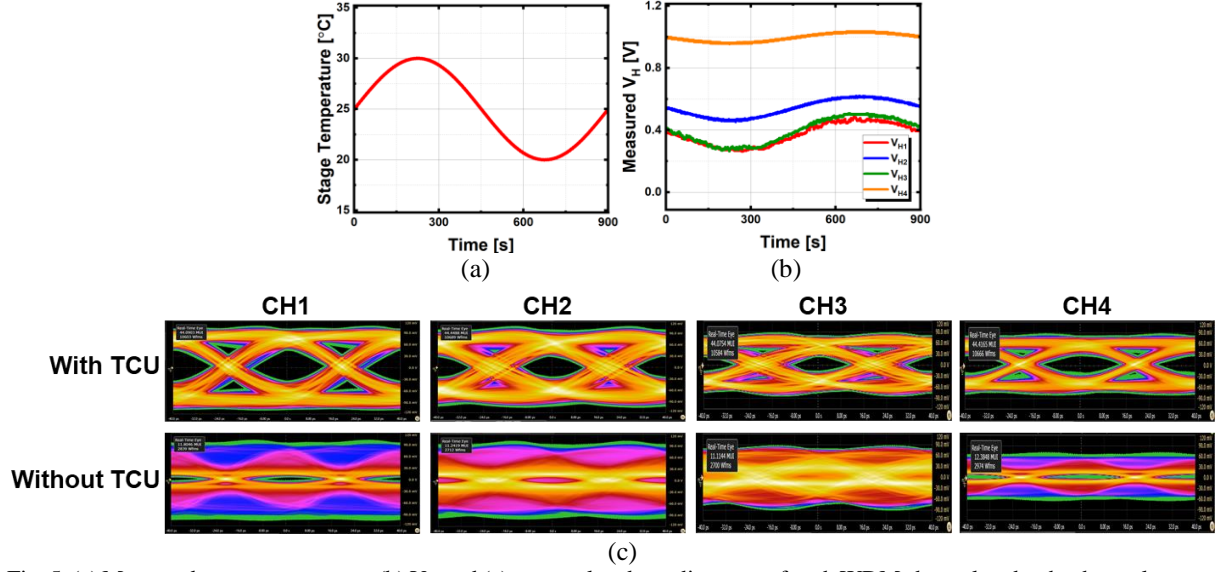


Fig. 5. (a) Measured stage temperature, (b) V_H and (c) accumulated eye diagrams of each WDM channel under the thermal stress.

To verify the stability of our technique, the thermal stress is applied by modulating the chip stage temperature for 900 seconds as shown in Fig. 5(a). Fig. 5(b) shows the measured V_H for each RRF heater in response to this thermal stress. Fig. 5(c) shows the accumulated eye diagrams of each WDM channel for the 25-Gb/s, PRBS-7 input data having an average power of -4-dBm during the thermal stress. As can be seen in the figure, the TCU can compensate for the thermal stress by properly changing the RRF heater voltages and maintain the good-quality eye diagram.

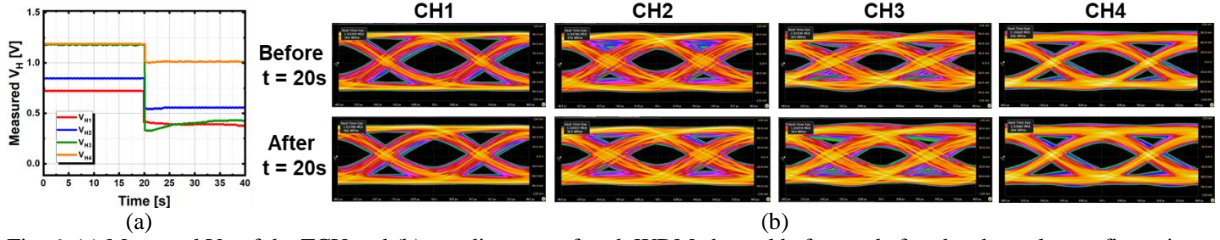


Fig. 6. (a) Measured V_H of the TCU and (b) eye diagrams of each WDM channel before and after the channel reconfiguration.

If there is a need for WDM channel reconfiguration, the TCU can easily determine the newly required heater voltages and apply them to RRF heaters. Fig. 6(a) shows the measured V_H when the channel reconfiguration is requested at $t = 20$ s. After the channel reconfiguration, dithering is executed to reduce the mismatch caused by the electrical heater crosstalk and process variation. Fig. 6(b) shows the eye diagrams of each WDM channel for the 25-Gb/s, PRBS-7 input data having an average power of -4-dBm before and after the channel reconfiguration. These measured results demonstrate the capability of our TCU for the WDM channel reconfiguration.

4. Conclusion

We present the reconfigurable fast wavelength locking calibration technique for the Si RRF-based WDM receiver with the FPGA-based TCU, which maintains calibration performance even with an increase in the number of WDM channels.

5. Acknowledgement

Jae-Ho Lee and Yongjin Ji contributed equally to this work. The authors are thankful to Samsung Electronics for chip fabrication, and to IC Design Education Center (IDEC) for EDA tool support. This work was supported by Samsung Advanced Institute of Technology under Grant IO201218-08228-01 and in part by IITP grant funded by the Korea Government under Grant RS-2023-00222171.

6. References

- [1] P. Bhargava *et al.*, "A 256Gbps Microring-Based WDM Transceiver with Error-Free Wide Temperature Operation for Co-Packaged Optical I/O Chiplets," in *Proc. IEEE Symp. VLSI Technol. Circuits*, Jun. 2024, pp. 1-2.
- [2] Z. Xuan *et al.*, "A 256 Gbps Heterogeneously Integrated Silicon Photonic Microring-Based DWDM Receiver Suitable for In-Package Optical I/O," in *Proc. IEEE Symp. VLSI Technol. Circuits*, Jun. 2023, pp. 1-2.
- [3] D. Oliveira *et al.*, "Automatic Tuning of Silicon Photonics Microring Filter Array for Hitless Reconfigurable Add-Drop," *J. Light. Technol.*, vol. 37, no. 16, pp. 3939–3947, Aug. 2019.
- [4] M. Georgas *et al.*, "Addressing Link-Level Design Tradeoffs for Integrated Photonic Interconnects," in *Proc. IEEE Custom Integr. Circuits Conf.*, Sep. 2011, pp. 1-8.
- [5] H.-K. Kim *et al.*, "A $4\text{-}\lambda \times 28\text{-Gb/s}/\lambda$ Silicon Ring-Resonator-Based WDM Receiver With a Reconfigurable Temperature Controller," *J. Light. Technol.*, vol. 42, no. 7, pp. 2296–2302, Apr. 2024.